Increasing the Signal-to-Noise Ratio in Underwater Distributed Optical Fiber Acoustic Sensor

Morteza Janfaza[a,*], Hamed Moradi[b], and Arsalan Jalil[b]

[a]Department of Electrical Engineering, Faculty of Engineering, University of Saravan, Saravan, Iran
[b]Faculty of Electrical Engineering, Sharif University of Technology, Tehran, Iran

Corresponding author email: m.janfaza@saravan.ac.ir

Regular Paper-Received: June 07, 2024, Revised: Sept. 30, 2024, Accepted: Oct. 02, 2024, Available Online: Oct. 04 , 2024
DOI: 10.61186/ijop.17.2.229

ABSTRACT— In this study, we present the findings derived from our simulation and experimental investigation of a distributed optical fiber acoustic sensor. The proposed sensor operates by utilizing the self-interference of Rayleigh backscattering. When the optical pulse propagates through the optical fiber, the phase of the Rayleigh backscattered light changes at the location where the acoustic signal is present. This phase change is then amplified through the self-interference of two Rayleigh backscattered beams in the Michelson interferometer scheme. This study aims to present the Phase Generated Carrier (PGC) demodulation method along with the arctangent function (ATAN) and the Coordinate Rotation Digital Computer (CORDIC) algorithm. This method offers a simple and efficient algorithm for computing hyperbolic and trigonometric functions. The system allows for the detection of acoustic waves caused by sinusoidal disturbances with a spatial resolution of approximately 20 m.

KEYWORDS: CORDIC algorithm, Distributed sensor, Interferometry, Modulus, Optical fiber acoustic sensor, Polymer.

I. INTRODUCTION

Optical fiber sensors involve the use of light guided through an optical fiber to interact with physical, chemical, and biological measurements. This interaction results in a modulated optical signal that carries information about the measurement parameter [1]-[3]. Fiber sensors have several advantages over conventional electronic sensors. These include their lightweight design, resistance to electromagnetic interference, high sensitivity, and multiplexing capability [1]-[3]. Optical fiber sensors can be classified into four main categories based on their properties: intensity-modulated, phase-modulated (interferometric), polarization-modulated (polarimetric), and wavelength-modulated (spectrometric) sensors.

Optical fiber sensors possess the ability to measure a wide range of physical, chemical, and biological quantities [4]-[15]. Distributed optical fiber sensors enable simultaneous measurement at thousands of points, using a standard, unmodified optical fiber as the sensing element. These sensors work by using both elastic and inelastic scattering in optical fibers. Specifically, when Rayleigh scattering is dominant, elastic scattering occurs. Distributed optical fiber sensor that utilizes Rayleigh scattering; scattering is used exclusively to monitor and detect propagation effects [16]-[20]. Recently, there have been some reports in which Rayleigh backscattering is employed to detect acoustic perturbations [5], [8]-[10], [16]-[18].

A distributed fiber-optic acoustic sensor can detect and locate single or multiple acoustic events occurring at any position of the fiber under test (FUT) [8]-[10]. These findings have promising applications in maintaining border intrusion, oil and gas pipeline security, and structural health. Currently, there have been numerous reports on interferometric optical fiber acoustic sensors. These reports describe

[Downloaded from ijop.ir on 2026-11-26]

different demodulation methods and interferometric configurations, such as Mach-Zehnder [21], [22], Michelson [23]-[25], and Fabry-Perot [26], [27]. The interferometer output is a cosine function that relies on the phase difference between its two arms. This phase difference can be affected by random temperature and pressure fluctuations, leading to signal fading or random changes in the detected signal [28]. The PGC demodulation method is desirable for reducing signal fading, as it offers high efficiency and good linearity. A recent study thoroughly explored different demodulation methods for interferometric optical fiber acoustic sensors, such as the CORDIC algorithm.

In this paper, we aim to simulate the acoustic demodulated signal of a distributed optical fiber acoustic sensor. The simulation is based on the self-interference of two Rayleigh backscattered beams, which are obtained from a Michelson interferometer. To accomplish this, we utilize the ATAN+CORDIC algorithm. The verification process involves creating a distributed optical fiber acoustic sensor. This sensor exploits the demodulated signal, which is obtained by integrating the PGC method with the ATAN+CORDIC algorithm. By digitally implementing the CORDIC algorithm on an FPGA, we achieve a consistent frequency response and an improved signal-to-noise ratio. This sensor is capable of detecting acoustic waves within the frequency range of 0.5-5 kHz. To the best of our knowledge, this is the initial endeavor to enhance sensitivity in a distributed optical fiber acoustic sensor through the utilization of two acousto-optic modulators (AOMs) and low-modulus polymeric materials. The results indicate that the utilization of polyvinyl chloride yields an improvement of 8 dB in the power spectrum of the sensor at 1 kHz, as opposed to the situation in the absence of polymeric packaging.

II. THEORY AND SIMULATION

Figure 1 illustrates the optical fiber path in the Michelson interferometer. The Faraday Rotator Mirror (FRM) is a fiber optic polarization rotation mirror designed for fiber optic networks and measurement applications. The FRM in Figs. 1 and 2 play the role of a mirror that is used to set up the Michelson interferometer. As shown in Fig. 1, ω_0 is the modulation frequency and S is the path difference between the two sensing arms. e_r is the electric field of the backscattered wave from the upper arm of the interferometer, and e_{rs} is the electric field of the backscattered wave from the lower arm of the sensor. When a coherent light pulse with a duration of W and an optical frequency of f is injected into a fiber at t=0, a backscattered wave is generated at the input end of the fiber. This backscattered wave can be mathematically represented as [19], [20]:

$$e_r(t) = \sum_{i=1}^{N} a_i \exp\left(-\alpha \frac{c\tau_i}{n_f}\right) \cos\left[2\pi f\left(t-\tau_i\right)\right] \mathrm{rec}\left(\frac{t-\tau_i}{W}\right) \quad (1)$$

where a_i and τ_i are the amplitude and delay of the backscattered wave, respectively, for the ith backscattering. N represents the total number of backscatterings.

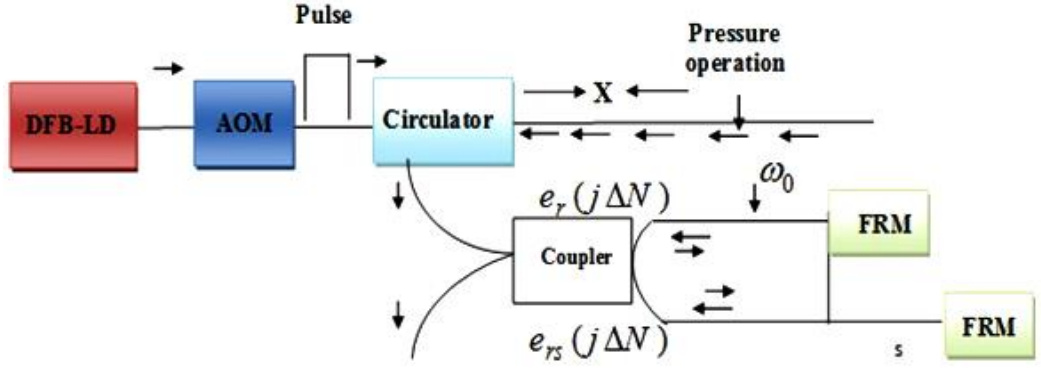


Fig. 1. Schematic illustrates the optical path in a Michelson interferometer, which incorporates a distributed feedback laser diode (DFB-LD), an acoustic-optic modulator (AOM), and a Faraday rotator mirror (FRM) [20].

[Downloaded from ijop.ir on 2026-11-26]

The rectangular function is provided as:

$$\begin{cases} \mathrm{rec}\left(\dfrac{t-\tau_i}{W}\right)=1 \quad \text{when} \quad 0<t-\tau_i<1 \\ \mathrm{rec}\left(\dfrac{t-\tau_i}{W}\right)=0 \quad \text{otherwise} \end{cases} \tag{2}$$

The relationship between distance z_i (from fiber input) and time delay τ_i is given by $\tau_i = 2n_f z_i / c$. The refractive index of the fiber is n_f, and the spectral resolution of the system is defined as $S_R = cW/2n_f$. The relationship between location accuracy, ΔN, and sampling rate, S_a, is defined as:

$$\Delta N = \frac{c}{2S_a n_f} \tag{3}$$

Equation 1 represents the distance, denoted as x, from the input end in the sensing fiber is written as:

$$e_r(x) = \sum_{i=1}^{N} a_i \exp\left(-2\alpha z_i \cos\left[\frac{4\pi f}{c}\times \times\left(x-z_i\right)\right]\right)\mathrm{rect}\left(\frac{x-z_i}{S_R}\right) \tag{4}$$

The complete details of the acquired relations for utilizing them in the data acquisition system are elaborated in [19], [20].

The PGC method is utilized for the detection of minute signal phase shifts, thereby mitigating signal fading resulting from significant environmental fluctuations. This is accomplished by introducing a high-amplitude phase shift at a frequency distinct from the signal band. These signals of interest are carried as sidebands by these significant amplitude signals. Equation 5 can be used to express the light intensity at the output of the interferometer [28]:

$$I = A + B\cos\left(C\cos\left(\omega_0 t\right)+\phi(t)\right) \tag{5}$$

where A and B are constants that represent the average intensity and visibility of the interferometer, respectively. Meanwhile, $C\cos\left(\omega_0 t\right)$ is a sinusoidal modulation with a frequency of ω_0 and an amplitude of C. This modulation is applied to one arm of the interferometer. The carrier signal can be generated using either a phase modulator or a piezo-electrically stretched fiber coil. This signal, $\phi(t)$, encompasses not only the desired signal but also various environmental effects, $\psi(t)$, Written by:

$$\phi(t) = D\cos(\omega t)+\psi(t) \tag{6}$$

The frequency and amplitude of the signal are determined by ω and D, respectively. By utilizing Bessel functions to expand Eq. 5, we can determine [28]:

$$I = A + B\left\{\left[J_0(C)+2\sum_{k=1}^{\infty}(-1)^k J_{2k}(C)\cos\cos\left(2k\omega_0 t\right)\right]\cos\phi(t) - \left[2\sum_{k=0}^{\infty}(-1)^k J_{2k+1}(C)\cos\cos\left((2k+1)\omega_0 t\right)\right]\sin\phi(t)\right\} \tag{7}$$

Similarly, by expanding the phase angle, $\phi(t)$, in Eq. 6, Eqs. 8 and 9 can be derived as [28]:

$$\cos\phi(t) = \left[J_0(D)+2\sum_{k=1}^{\infty}(-1)^k J_{2k}(D)\cos\cos\left(2k\right)\omega t\right]\cos\psi(t) - \left[2\sum_{k=0}^{\infty}(-1)^k \times J_{2k+1}(C)\cos\cos\left(2k+1\right)\omega t\right]\sin\psi(t) \tag{8}$$

[Downloaded from ijop.ir on 2026-11-26]

$$\sin\phi(t)=\left[2\sum_{k=0}^{\infty}(-1)^{k}J_{2k+1}(D)\right.$$
$$\left.\cos\cos(2k+1)\omega t\right]\cos\psi(t)-\left[J_{0}(D)\right. \quad (9)$$
$$\left.+2\sum_{k=1}^{\infty}(-1)^{k}J_{2k}(D)\cos\cos(2k)\omega t\right]\sin\psi(t)$$

The Bessel functions mentioned in Eqs. 7-9 are denoted as $J_n(C)$ and $J_n(D)$. The PGC demodulation method is employed during the simulation and experimental investigation, which is based on the ATAN+CORDIC algorithm [26].

III. Experimental Setup and Results

Figure 2 illustrates the experimental setup. A 1550nm DFB-LD from NKT Photonics, with a narrow linewidth of around 5kHz, generates a power of 8mW. This power is then increased to 300mW using an Erbium-doped fiber amplifier (EDFA). To eliminate the amplified spontaneous emission (ASE) noise produced by the EDFA, a narrowband pass filter is used. The amplified light is modulated using one or two AOMs to generate a 200 ns pulse with a repetition rate of 100 kHz. This repetition rate corresponds to a sensing length of 1km, considering the time it takes for light to propagate through the fiber. AOM also causes a frequency shift of 100 MHz, which is performed using an RF driver and a function generator (FG). Next, circulator one is used to launch the optical pulse into the fiber under test. The FUT is comprised of three sections of standard single fiber, including a 500m optical fiber, a 20m optical fiber wound around a disk PZT, and a 470m optical fiber. The resonance frequency of the PZT is set at 36 kHz. The sinusoidal waves ranging from 0.5 to 5 kHz with a peak-to-peak value of 5 are applied to the PZT throughout a series of experiments. An underwater speaker and a 20m optical fiber wound around a disk PZT are fixed in the tank. The water tank is used in the initial test for the possibility of obtaining a signal in a water environment. In the next step, we plan to conduct the test in a larger environment, such as a water pool. In fact, the data acquisition system is to be adapted to the water environment.

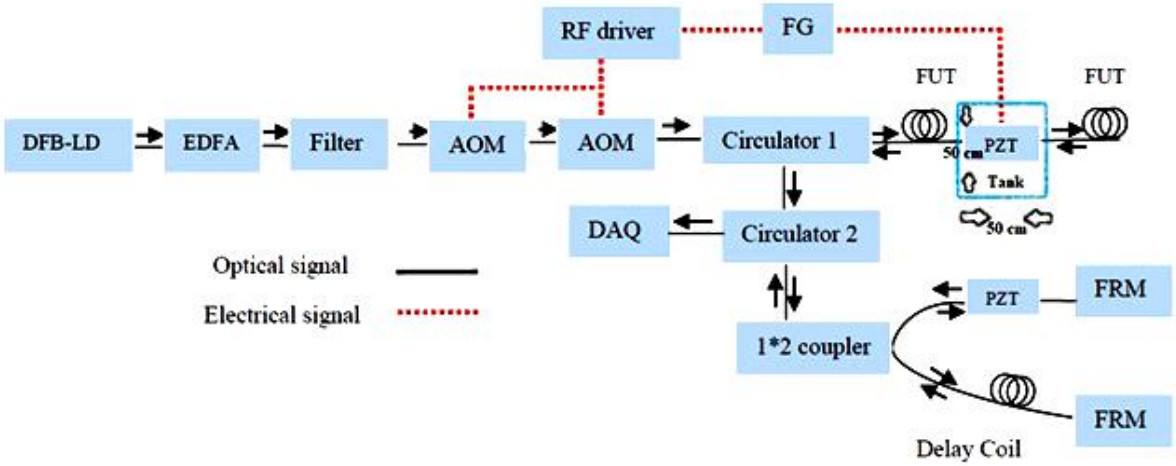


Fig. 2. The experimental setup of a distributed optical fiber sensor includes several components: a distributed feedback laser diode (DFB-LD), an erbium-doped fiber amplifier (EDFA), a bandpass filter, an acoustic-optic modulator (AOM), a circulator, a coupler, a Faraday rotator mirror (FRM), a delay coil, a fiber under test (FUT), a function generator (FG), a radio frequency (RF) driver, a piezoelectric transducer (PZT), and a data acquisition system (DAQ).

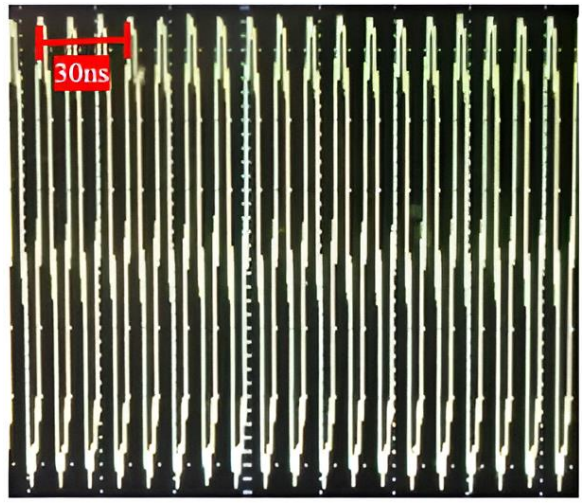
The Rayleigh backscatter signal was transmitted into the Michelson interferometer through circulator two and a 3 dB 1×2 coupler. When an acoustic pressure interacts with the fiber, it causes a phase alteration in the Rayleigh backscatter signal. Significant phase changes in the fiber are primarily attributed to variations in its length rather than changes in

[Downloaded from ijop.ir on 2026-11-26]

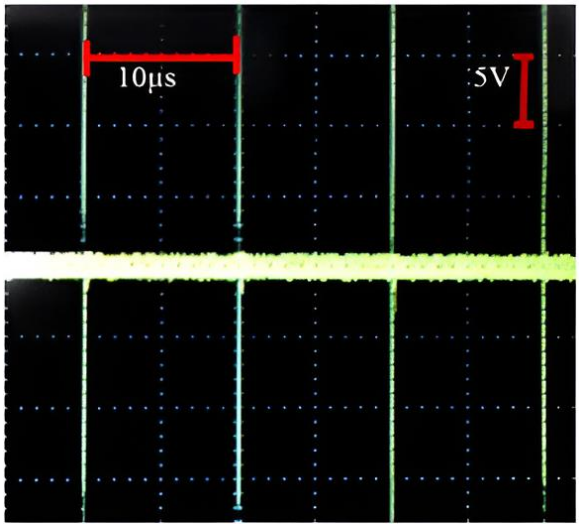
the refractive index. In the setup of the interferometer, one arm is utilized as a delay line through the use of a delay coil. In contrast, the other path is subjected to modulation by a phase modulator (PM) operating at a frequency of 36 kHz. The optical path imbalance, which is specified to have a spatial resolution of 20 m, is determined by the pulse width of 200 ns. The modulated light is interfered with by the delayed light at the 3dB coupler. Subsequently, this interfering light is received by a photoelectric detector (PD). The PD has a dark current of 2 nA and a responsivity of 0.9 A/W. The output of the PD is then collected using a 200 MHz oscilloscope with a sampling rate of 2 GSa/s. The PGC module in the data acquisition system (DAQ) is responsible for demodulating the phase information in Rayleigh backscattering. Figure 3 illustrates the RF driver output in both continuous wave (CW) and pulsed mode. As depicted, the RF driver generates a 100MHz output with a maximum amplitude of 17.2 V.

In the pulsed version, the CW is modulated by using a function generator with a repetition rate of 100 kHz. Figure 4 illustrates the power spectrum of the demodulated signal obtained from the sensor output at various frequencies for a specific AOM configuration. The results indicate a significant power spectrum at different frequencies when the ATAN+CORDIC algorithm is employed. The CORDIC algorithm achieves a maximum power of -25 dB at 0.5 kHz, with additional peaks at -25.5 dB, -27.5 dB, -30.5 dB, -29.5 dB, and -26 dB at 1 kHz, 2 kHz, 3 kHz, 4 kHz, and 5 kHz, respectively. The acoustic waves are obtained within the frequency range of 0.5 kHz to 5 kHz, effectively filtering out the harmonic frequencies of the phase modulation.

One of the main factors contributing to noise in distributed optical fiber sensors is AOM noise. This type of noise is primarily caused by the low extinction ratio of the AOM. In our experimental setup, we have utilized two AOMs. As shown in Fig. 5, the signal-to-noise ratio (SNR) for frequencies of 0.5 kHz, 1 kHz, 2 kHz, 3 kHz, 4 kHz, and 5 kHz is 23 dB, 25 dB, 20 dB, 18 dB, 20 dB, and 23 dB, respectively, when one AOM is used in the setup.



(a)



(b)

Fig. 3. (a) CW output of RF driver at 100 MHz and (b) modulated output of RF driver by FG at 100 kHz. This pulse repetition rate is equivalent to a 1 km sensing length considering the propagation time of light through the fiber.

By utilizing two AOMs, the extinction ratio of the AOMs complex is naturally enhanced. Consequently, the noise is reduced and the SNR is increased, as depicted in Fig. 5. With the increase in the SNR ratio, the system's mechanics are changed, and polymer materials are placed on the optical fiber at certain lengths of the sensing fiber. Each data point in Fig. 5 corresponds to the average of ten measurements. The error bar in Fig. 5 signifies the standard deviation of the results for each data point at different frequencies.

[Downloaded from ijop.ir on 2026-11-26]

Figure 5 (green points) illustrates the fast Fourier transform (FFT) findings of the demodulated signal for the ATAN+CORDIC algorithm experimental results of the two AOMs setup. The fluctuation of the frequency response of the sensor is also recorded at about 7 dB, promising a nearly flat frequency response.

The FUT additionally employs various polymers for packaging at the site where the acoustic signal is applied. The packaging has dimensions of 10 cm in length, 3 cm in width, and 1 mm in thickness.

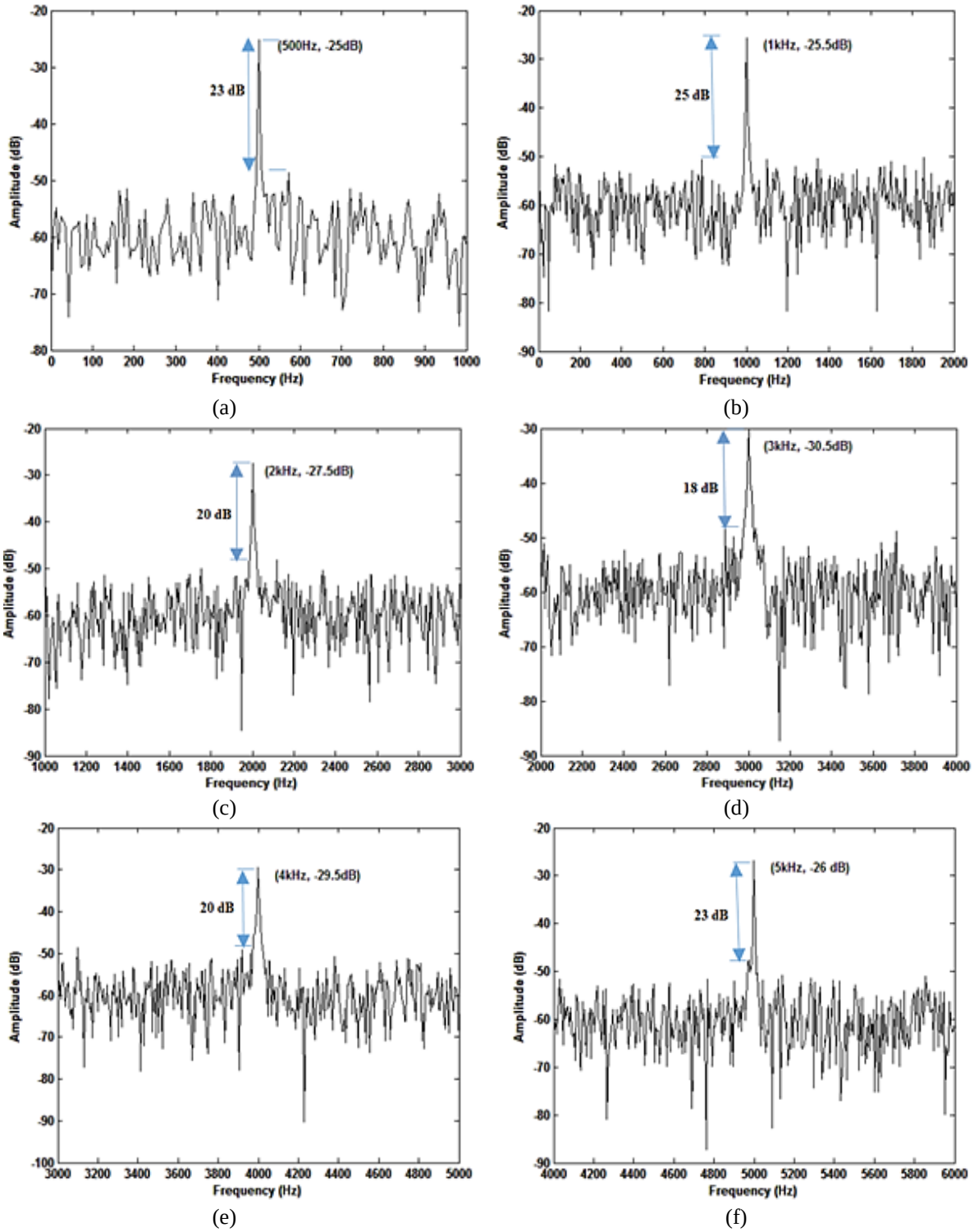


Fig. 4. Experimental demodulated acoustic signal obtained by the ATAN and ATAN+CORDIC algorithms using DAQ at (a) 0.5 kHz, (b) 1 kHz, (c) 2 kHz, (d) 3 kHz, (e) 4 kHz, and (f) 5 kHz for setup including one AOM.

[Downloaded from ijop.ir on 2026-11-26]

Figure 6 illustrates the impact of these polymers on sensor sensitivity. The results clearly indicate that the presence of polymers enhances the overall sensitivity of the acoustic sensor. When an acoustic event takes place, the sensor detects the pressure exerted by the acoustic wave on the elastic polymer layers, such as polyurethane, soft polyvinyl chloride, or polyethylene. This has a profound impact on the stress within the optical fiber, leading to deformation and a substantial alteration in its length. Additionally, the changes in modulus also influence the length of the fiber, thereby inducing variations in the optical phase shift in response to the acoustic signal. When the acoustic signal is applied, the lower modulus of the polymer results in a more pronounced change in the length of the optical fiber. The table below presents the respective moduli of the polymers employed (Table 1). Note that soft polyvinyl chloride has the lowest modulus compared to other polymers. Each experimental data point represents the average of ten different measurements. The error bar assigned to each data point reflects the standard deviation of the results at the corresponding frequency.

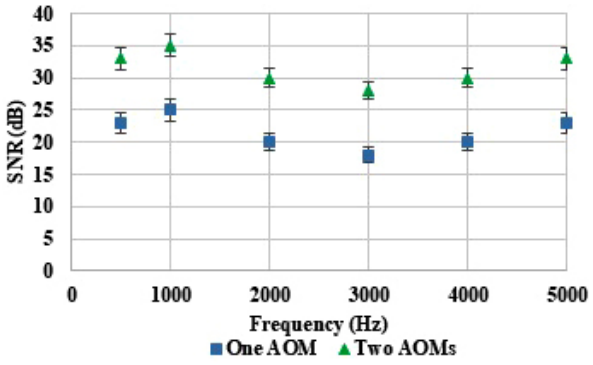


Fig. 5. SNR of distributed optical fiber acoustic sensor for one AOM and two AOMs setup.

Table **1** The Young modulus of different polymers

Polymer	Value
Polyurethane	A few hundred of MPa
Soft polyvinyl chloride	A few tens of MPa
Ployethylene	A few GPa

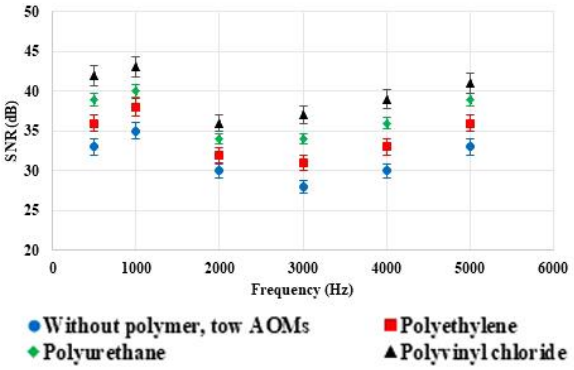


Fig. 6. SNR of a distributed optical fiber acoustic sensor for a homemade sensor with different polymeric packaging.

Table 2 compares the important advantages and features in this work with other structures.

Table 2. Comparison with different works

Reference	Important advantage and feature
[29]	Significant sensing length
[30]	High spatial resolution
[19]	Significant sensing length using amplifier
This Work	Using polymer materials to improve sensitivity, using the Cordic algorithm to facilitate hardware implementation

IV. CONCLUSION

This paper deals with the demodulated signal of a distributed acoustic sensing system. Research has demonstrated the ability to identify and separate an acoustic signal from ambient background noise. A distributed optical fiber acoustic sensor is implemented with the ATAN+CORDIC algorithm for the first time. The simple digital implementation of the CORDIC algorithm on FPGA is a significant advantage of this algorithm. Results from FFT plots also reveal that the PGC ATAN method using the CORDIC algorithm benefits from a good signal-to-noise ratio, characterizing a flat frequency response. Furthermore, the experiment's findings exemplify the potential for detecting the standard sinusoidal wave across a frequency range of 0.5-5 kHz when it is applied to the PZT location. The results emphasize that using soft polyvinyl chloride packaging around the FUT significantly increases the power spectrum of the sensor.

[Downloaded from ijop.ir on 2026-11-26]

REFERENCES

G. Rajan, Introduction to optical fiber sensors Optical Fiber Sensors: Advanced Techniques and Applications, Rajan, G., Iniewski, K., Eds, p. 1, 2015.

K. Grattan and B. Meggitt, Optical fiber sensor technology: advanced applications-Bragg gratings and distributed sensors, Springer Science & Business Media, 2000.

E. Udd and W.B. Spillman Jr, Fiber optic sensors: an introduction for engineers and scientists, 3rd ed., John Wiley & Sons, 2024.

Y. Zhang, D. Feng, Z. Liu, Z. Guo, X. Dong, K. Chiang, and B.C. Chu, "High-sensitivity pressure sensor using a shielded polymer-coated fiber Bragg grating," IEEE Photon. Technol. Lett., Vol. 13, no. 6, pp. 618-619, 2001.

F. Wang, X. Zhang, X. Wang, and H. Chen, "Distributed fiber strain and vibration sensor based on Brillouin optical time-domain reflectometry and polarization optical time-domain reflectometry," Opt. Lett., Vol. 38, no. 14, pp. 2437-2439, 2013.

A. Masoudi, M. Belal, and T.P. Newson, "Distributed optical fibre audible frequency sensor," 23rd International Conference on Optical Fibre Sensors, Vol. 9157: SPIE, pp. 537-540, 2014.

A. Owen, G. Duckworth, and J. Worsley, "OptaSense: Fibre optic distributed acoustic sensing for border monitoring," European Intelligence and Security Informatics Conference, IEEE, pp. 362-364, 2012.

D. Chen, Q. Liu, and Z. He, "Phase-detection distributed fiber-optic vibration sensor without fading-noise based on time-gated digital OFDR," Opt. Express, Vol. 25, no. 7, pp. 8315-8325, 2017.

G. Tu, X. Zhang, Y. Zhang, F. Zhu, L. Xia, and B. Nakarmi, "The Development of an φ-OTDR System for Quantitative Vibration Measurement," IEEE Photon. Technol. Lett., Vol. 27, no. 12, pp. 1349-1352, 2015.

M. Janfaza, H. Moradi, and M. Maleki, "Investigation of 2D materials effect on few-mode fiber optical temperature and strain sensors," Int. J. Opt. Photon., Vol. 15, no. 2, pp. 167-178, 2021.

M. Moccia, M. Consales, A. Iadicicco, M. Pisco, A. Cutolo, V. Galdi, and A. Cusano, "Resonant hydrophones based on coated fiber Bragg gratings," J. Lightwave Technol., Vol. 30, no. 15, pp. 2472-2481, 2012.

P.M. Junghare, C.P. Raj P, T. Srinivas, and P. Sharan, "A Finite Element Analysis of Fiber Optic Acoustic Sensing Mandrel for Acoustic pressure with Increased Sensitivity," Am. J. Eng. Research, Vol. 2, no. 9, pp. 1-7, 2013.

D. Passaro, M. Foroni, F. Poli, A. Cucinotta, S. Selleri, J. Laegsgaard, and A.O. Bjarklev, "All-silica hollow-core microstructured Bragg fibers for biosensor application," IEEE Sensors J., Vol. 8, no. 7, pp. 1280-1286, 2008.

A. Leung, P.M. Shankar, and R. Mutharasan, "A review of fiber-optic biosensors," Sensors Actuators B: Chem., Vol. 125, no. 2, pp. 688-703, 2007.

O. Wolfoeis, Fibre Optic Chemical Sensors, Vols. I & II, ed: CRC Press Boca Raton, FL, 1991.

Q. Chen, C. Jin, Y. Bao, Z. Li, J. Li, C. Lu, L. Yang, and G. Li, "A distributed fiber vibration sensor utilizing dispersion induced walk-off effect in a unidirectional Mach-Zehnder interferometer," Opt. Express, Vol. 22, no. 3, pp. 2167-2173, 2014.

S. Liang, X. Sheng, S. Lou, P. Wang, and Y. Zhang, "Novel Lissajous figure-based location method for fiber-optic distributed disturbance sensor," Int. J. Light Electron Opt. (Optik), Vol. 126, no. 23, pp. 4362-4366, 2015.

H.F. Martins, S. Martin-Lopez, P. Corredera, M.L. Filograno, O. Frazao, and M. Gonzalez-Herráez, "Phase-sensitive optical time domain reflectometer assisted by first-order Raman amplification for distributed vibration sensing over> 100 km," J. Lightwave Technol., Vol. 32, no. 8, pp. 1510-1518, 2014.

Y. Shang, Y. Yang, C. Wang, X. Liu, C. Wang, and G. Peng, "Optical fiber distributed acoustic sensing based on the self-interference of Rayleigh backscattering," Measurement, Vol. 79, pp. 222-227, 2016.

Y. Shang, Y.-H. Yang, C. Wang, X.-H. Liu, C. Wang, and G.-D. Peng, "Study on demodulated signal distribution and acoustic pressure phase sensitivity of a self-interfered distributed acoustic sensing system," Measurement Sci. Technol., Vol. 27, no. 6, pp. 065201(1-9), 2016.

N. Lagakos, T. Hickman, P. Ehrenfeuchter, J. A. Bucaro, and A. Dandridge, "Planar flexible fiber-optic acoustic sensors," J. Lightwave Technol., Vol. 8, no. 9, pp. 1298-1303, 1990.

G. Hocker, "Fiber-optic acoustic sensors with increased sensitivity by use of composite structures," Opt. Lett., Vol. 4, no. 10, pp. 320-321, 1979.

M. Imai, T. Ohashi, and Y. Ohtsuka, "Fiber-optic Michelson interferometer using an optical power divider," Opt. Lett., Vol. 5, no. 10, pp. 418-420, 1980.

X. Hong, J. Wu, C. Zuo, F. Liu, H. Guo, and K. Xu, "Dual Michelson interferometers for distributed vibration detection," Appl. Opt., Vol. 50, no. 22, pp. 4333-4338, 2011.

H. Moradi, F. Hosseinibalam, and S. Hassanzadeh, "Simulation and experimental investigation about interferometric optical fiber acoustic sensor for sensitivity enhancement," Measurement, Vol. 137, pp. 556-561, 2019.

H. Moradi, F. Hosseinibalam, and S. Hassanzadeh, "Improving the signal-to-noise ratio in a fiber-optic Fabry–Pérot acoustic sensor," Laser Phys. Lett., Vol. 16, no. 6, pp. 065106(1-8), 2019.

H. Moradi, P. Parvin, F. Shahi, and A. Ojaghloo, "Fiber optic Fabry–Pérot acoustic sensor using PVC and GO

[Downloaded from ijop.ir on 2026-11-26]

diaphragms," OSA Continuum, Vol. 3, no. 4, pp. 943-951, 2020.
A. Dandridge, A.B. Tveten, and T.G. Giallorenzi, "Homodyne demodulation scheme for fiber optic sensors using phase generated carrier," IEEE Trans. Microwave Theory Tech., Vol. 30, no. 10, pp. 1635-1641, 1982.
A. Masoudi, M. Beresna, and G. Brambilla, "152 km-range single-ended distributed acoustic sensor based on inline optical amplification and a micromachined enhanced-backscattering fiber," Opt. Lett., Vol. 46, no. 3, pp. 552-555, 2021.
A. Masoudi and T.P. Newson, "High spatial resolution distributed optical fiber dynamic strain sensor with enhanced frequency and strain resolution," Opt. Lett., Vol. 42, no. 2, pp. 290-293, 2017.



Morteza Janfaza received his B.Sc., M.Sc., and Ph.D. degrees in Electrical Engineering from the University of Sistan and Baluchestan, Zahedan, Iran, in 2011, 2013, and 2019, respectively. He is currently a member of the Engineering Faculty of University of Saravan. His current research interests include graphene, nano-optics, plasmonics, optoelectronic devices, nanoelectronics, and sensors.



Hamed Moradi received his PhD in Physics from the University of Isfahan in 2019. He is currently working as a researcher at Sharif University of Technology. His field of activity is fiber optic sensors and semiconductor optics.



Arsalan Jalil received his B.Sc. degree in electrical engineering and computer engineering (Minor) from Yazd University, Yazed, Iran, in 2019, and the M.Sc. degree in electrical engineering from Sharif University of Technology, Tehran, Iran, in 2023. He is currently working as a researcher at Sharif University of Technology. His field of activity is quantum computing and quantum Machine Learning, data Accelerator.

[Downloaded from ijop.ir on 2026-11-26]